Geomorphology 123 (2010) 165–180

Contents lists available at ScienceDirect

Geomorphology

journal homepage: www.elsevier.com/locate/geomorph

Gravitationally induced caves and other discontinuities detected by 2D electrical resistivity tomography: Case studies from the Polish Flysch Carpathians

Tomáš Pánek [a,*], Włodzimierz Margielewski [b], Petr Tábořík [a], Jan Urban [b], Jan Hradecký [a], Czesław Szura [c]

[a] Department of Physical Geography and Geoecology, Faculty of Science, University of Ostrava, Chittussiho 10, 710 00 Ostrava, Czech Republic
[b] Institute of Nature Conservation, Polish Academy of Sciences, al. Mickiewicza 33, 31-120 Kraków, Poland
[c] Association for the Caves Conservation "Malinka Group", ul. Fiedorowska 66, 43-460 Wisła, Poland

ARTICLE INFO

Article history:
Received 1 May 2010
Received in revised form 10 July 2010
Accepted 18 July 2010
Available online 24 July 2010

Keywords:
2D electrical resistivity tomography
Electrode array
Crevice-type caves
Slope deformations
Mass movements
Polish Flysch Carpathians

ABSTRACT

Widened discontinuities (among them crevice-type caves) are characteristic phenomena of landslides in anisotropic rock massifs forming the Flysch Carpathians. We tested the reliability of 2D electrical resistivity tomography (ERT) in the detection of well-mapped cave passages and then tried to explore new subsurface cavities in three sites of crevice-type caves in the Polish Flysch Carpathians: the Jaskinia Miecharska, Jaskinia Malinowska and Jaskinia Diabla Dziura caves; each comprising a different stage of mass-movement development and thus being a representative case study. The total of 14 ERT profiles was selected, while each of them was measured by several electrode arrays (dipole–dipole, Wenner and/or Wenner–Schlumberger). Our results show that the selection of an appropriate electrode array and spacing are crucial for the detection of subsurface cavities. Measurement using the dipole–dipole electrode array gave best results in the detection of known structures and its interpretation seems to be most reliable in the extrapolation of non-investigated areas. The application of ERT shows abundant occurrence of air-filled voids in gravitationally deformed flysch massifs and in several places its results enable comparison with open spaces detected by speleological exploration. ERT enables us to identify fractures in deformed slopes before the proper failure of these slopes affected by a landslide as well as in landslides themselves: fissure zones connected with trenches, less dense segments of colluvial ramparts and some lithological-tectonical or gravitationally induced elements of slope structures. The reliability of ERT detection of potential caves was verified by speleological exploration of a newly discovered cave at the Jaskinia Miecharska site following the ERT campaign.

1. Introduction

Near-surface geophysical methods have recently become an important tool in geomorphological research (Schrott and Sass, 2008). One of the most frequently used geophysical techniques is electrical resistivity tomography (ERT; also named DC resistivity). This geoelectrical method offers quick and cost-effective imaging of subsurface resistivity pattern to a depth of several tens of meters. In combination with other geophysical techniques (e.g. ground penetration radar and seismic refraction), ERT provides a reliable model of subsurface structures and thus improves the interpretation of landform evolution (e.g. Bichler et al., 2004; Godio et al., 2006; Sass, 2006; Ganerød et al., 2008; Sass et al., 2008).

In recent years, ERT application has become the focus of studies dealing with active fault detections (Suzuki et al., 2000; Nguyen et al., 2007; Fazzito et al., 2009); internal structure and depth of landslides (Lapenna et al., 2003; Bichler et al., 2004; Drahor et al., 2006; Jomard et al., 2007; Schrott and Sass, 2008); thickness of surficial deposits (Zhou et al., 2000; Maillet et al., 2005; Otto and Sass, 2006; Sass, 2006; Beauvais et al., 2007); and mountain permafrost analyses (Kneisel, 2006; Ribolini et al., 2010). Although potentially feasible, much less attention has been paid to geomorphic problems connected with the presence of air-filled subsurface voids like karst caves (Abu-Shariah, 2009; Guérin et al., 2009) or mechanically induced underground cavities (Chambers et al., 2007).

On an example of pseudokarst, mainly crevice-type caves in the Polish Flysch Carpathians, our study aims to present possibilities of the application of ERT in the detection of widened crevices and discontinuities occurring in deep-seated (>30 m according to Hutchinson, 1995) and intermediate (10–30 m) gravitational slope deformations. According to our findings, it is the first extensive test of 2D electrical resistivity profiling of such phenomena connected with gravitational mass movements. Pseudokarst (non-karst) caves are common features in anisotropic rock massifs of the Outer Flysch Carpathians (Wagner et al., 1990; Pulina, 1997a,b; Margielewski and

* Corresponding author. Tel.: +420 597 092 306; fax: +420 597 092 323.
E-mail address: tomas.panek@osu.cz (T. Pánek).

0169-555X/$ – see front matter © 2010 Elsevier B.V. All rights reserved.
doi:10.1016/j.geomorph.2010.07.008

Urban, 2003a, 2005). In comparison with karstic caves, pseudokarst caves are usually much narrower and significantly elongated in vertical direction. They are typical elements of gravitationally modified slopes accompanied by other gravitational-induced landforms like ridge-top trenches, counter-slope scarps and sinkholes. These landform assemblages are even major landscape elements in some parts of the Flysch Carpathians (Margielewski, 2006) and detailed investigation of their genesis is crucial for better understanding the evolution of medium–high mountains in the Carpathian flysch belt.

The possibility to compare results of the ERT method with the existing subsurface discontinuities (accessible as caves) and surface slope deformations studied in details creates a unique opportunity (i) to test the method, (ii) to investigate the subsurface structures and, in consequence, (iii) to understand better the processes affecting mountain slopes. Accordingly, the aims of our paper are (i) to demonstrate geoelectrical evidence of known crevice-type caves and other mass-movement-related discontinuities, (ii) to test the reliability of ERT in the detection of potential pseudokarst caves, (iii) to reveal differences in the displaying of subsurface structures when using various electrode spacing and arrays and (iv) to try to evaluate the ERT record in order to improve a model of slope failure evolution in anisotropic flysch massifs.

2. Regional settings

The Outer (Flysch) Carpathians, also called the Beskidy Mountains (in Polish language), represent Alpine orogene built by Late Jurassic to Early Miocene siliciclastic-clayey flysch rocks. These rocks were tectonically framed in the Neogene, forming several tectonic-facies units (nappes) that thrust one over another in a northward direction. The following units are distinguished in the region (from the south): Magura Unit, Dukla Unit (and their equivalents), Silesian Unit, Sub-Silesian Unit and Skole Unit. Folded Miocene deposits form two units: Stebnik Unit (northeastern part) and Zgłobice Unit (northern part of the Polish Carpathians) (Fig. 1). The northern foreland of the Polish Flysch Carpathians is occupied by the Carpathian Foredeep built by Miocene formations (Żytko et al., 1989; Lexa et al., 2000).

The Beskidy Mountains and their Foothills are divided into many ranges (mountain groups), which rise from several tens of metres up to 800 m above the stream and river valleys separating them (Starkel, 1972). Steep slopes of these mountain ranges are mainly covered by forests and during the Holocene they were predominantly shaped by gravitational mass movement. The development of gravitational mass movement such as landslides, toppling or lateral spreading has been facilitated by geological structure of slopes, e.g. by the alternation of thick-bedded sandstones–conglomerates and shales and/or thin-bedded sandstone–shale series and by the presence of densely jointed rocks. These preparatory factors were favourable for the disturbance of slope equilibrium caused by external factors: fluvial erosion, water overloading of rocks and earthquakes often occurring in the region (e.g. Bober, 1984; Zabuski et al., 1999; Poprawa and Rączkowski, 2003; Margielewski, 2006).

Gravitational evolution of slopes is a prolonged process starting with gradual and slow spreading or toppling of a massif and ending with rapid formation of a landslide. The propagation and subsequent widening of a system of rock discontinuities is a basic element of the initial, preparatory stage of landslide development. Widened crags controlled by structural elements such as joints and faults are pseudokarst phenomena, and if accessible to people, they are classified as crevice-type caves (Vítek, 1983; Margielewski and Urban, 2002, 2003a,b). Another genetic-structural type of pseudokarst caves is directly connected with landslide formation and it represents voids formed between translated and rotated rock blocks displaced during rapid mass movement (most of them belong to talus-type caves according to the classification of Vítek, 1983).

Both types of caves are very common in the Beskidy Mts and more than 1000 of them have been found and explored in this region. Jaskinia Wiślańska, the largest cave in the Beskid Śląski Mts, is 2275 m long and 41 m deep (Szura, 2009); 34 others are more than 100 m long (Klassek and Mleczek, 2009). All long caves are related to landslides or are situated in slopes that are undergoing the initial stage of gravitational evolution. The study sites (Fig. 1) show surface and underground features typical of various stages of gravitational slope deformation:

- initial slope transformation with subsurface forms preceding the landslide development—Jaskinia Malinowska cave;
- a rotational landslide with typical but deep propagation of the gravitational unloading stress zone—Diabla Dziura cave;
- a complex type of a landslide with large and multistage landforms and subsurface voids—Jaskinia Miecharska cave.

2.1. Jaskinia Malinowska cave

The Jaskinia Malinowska cave (MAC) is situated in the western slope of Mt Malinów (1116 m a.s.l) in the Beskid Śląski Mts (Fig. 1),

Fig. 1. Geological map of the Polish Carpathians showing the location of analyzed sites: 1—Jaskinia Malinowska Cave site; 2—Diabla Dziura Cave site; 3—Jaskinia Miecharska Cave site.

namely in the Upper Godula beds (Upper Cretaceous), which occur in the sequence of the Silesian Unit (Burtan, 1973; Ryłko and Paul, 1992). In this part the Upper Godula, beds are composed of very thickly bedded sandstones and conglomerates (Malinów Conglomerate) slightly inclined to the south and southwest and involving rare inserts of shales (Fig. 2) (Margielewski and Urban, 2002, 2003a).

The cave is situated in the upper part of the slope, close to the summit of the massif. At this point the slope has not been destroyed by a landslide yet; however, the cave itself and small surface depressions situated west off the cave (Fig. 2) evidence the process of the gravitational destruction of slope preceding rapid mass movements. The MAC is 245.5 m long and up to 19.5 m deep (Klassek and Mleczek, 2009). The main part of the cave is composed of an array of high (up to 15 m), rather narrow (0.5–2 m) and 2–20 m long galleries, rectangular in transversal cross section (Pulina, 1997a). These galleries are widened fissures representing two complementary joint sets of a diagonal system: $D_1 = 300–310°$ and $D_2 = 20–25°$. They were formed due to the process of dilatation (dilation) defined as "deformation by a change in

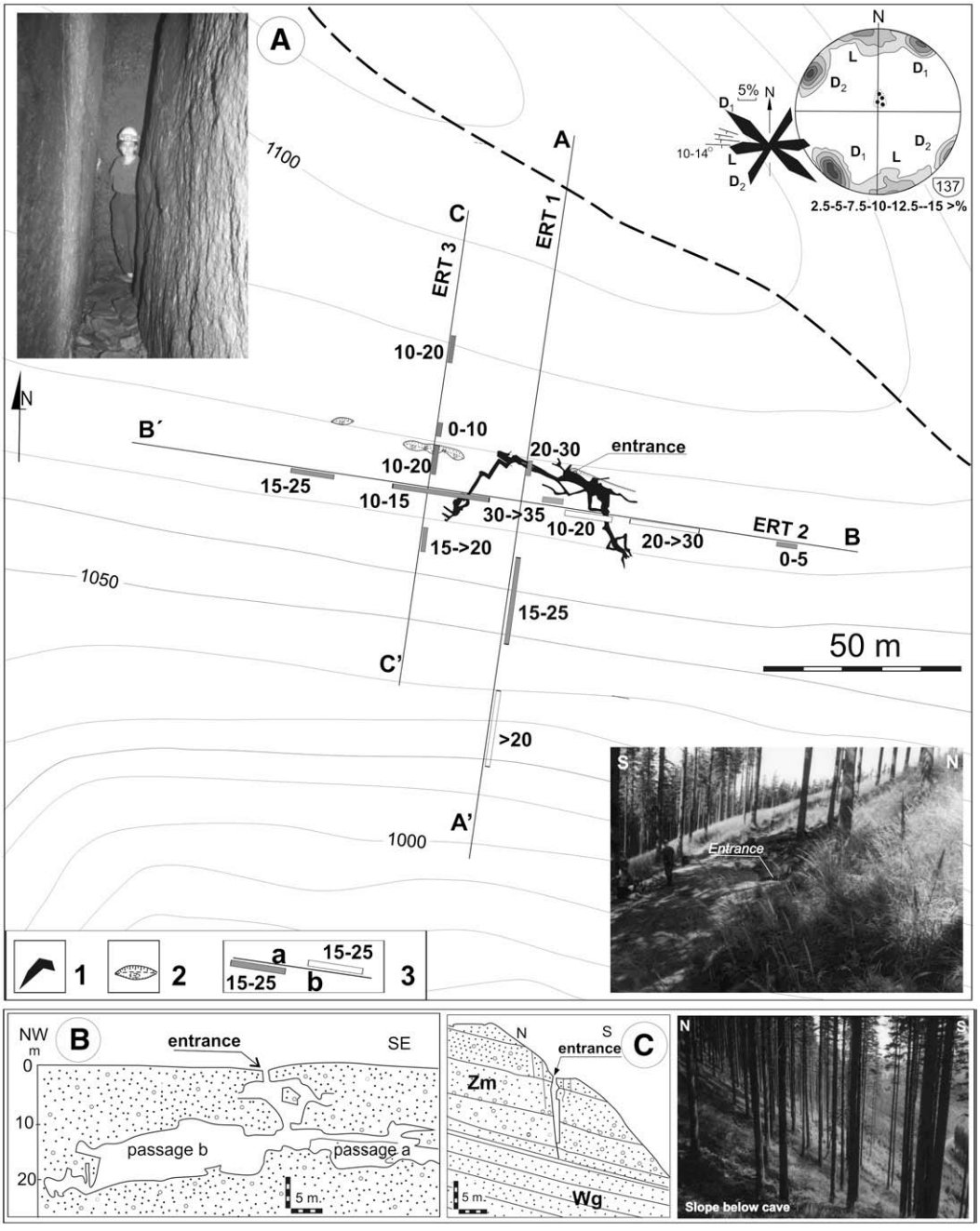

Fig. 2. Jaskinia Malinowska Cave site. (A) Map of the cave (simplified after Rachwaniec 1997) and its surroundings. Explanation of symbols in the legend: 1—cave, 2—surface depression, 3—ERT profile with marked high-resistivity anomalies: a—apparent high-resistivity signal and its depth in meters, b—less apparent high-resistivity signal and its depth in meters; steeply dipping ERT profiles are shortened according to their projection on horizontal plane. Joints in rose and contour diagrams—equal area plot, projection of poles in the lower hemisphere, with the number of measurements and contour intervals; joint sets: L—longitudinal, T—transversal; D_1, D_2—diagonal. Bedding plane in the pole point diagram (projection in the lower hemisphere). Upper left photo—cave passage. Lower right photo—cave entrance. (B) Longitudinal cross section of the cave (simplified after Ganszer 1997). (C) Conceptual model of transversal cross section of the cave and geological structure (modified after Margielewski and Urban, 2003a). Zm—sandstone and conglomerate, Wg—sandstone and shale. Photo—slope below the cave.

volume but not shape". The longest passage situated in the central part of the cave is parallel to the slope contours, whereas both side (left and right) passages are bent towards the slope (Fig. 2). The cave thus practically reflects the form of a prospective landslide scar of a circular shape (Margielewski and Urban, 2003a).

2.2. Diabla Dziura cave

The Diabla Dziura cave (DIC) is situated in the range of Mt Bukowiec (ca. 500 m a.s.l.) in the Rożnów Foothill of the Beskidy Mts (Fig. 1). In geological terms, it is formed in the Ciężkowice beds (Palaeocene–Eocene) of the Silesian Unit. The Ciężkowice beds are composed of very thick-bedded, mainly coarse-grained sandstones with rare inserts of shales and thinly bedded flysch (Cieszkowski et al., 1991). The strata are slightly inclined to the south (SSW) building a hill range stretching in the WSW–ENE direction and steeply sloping to the north. Two generations of landslides with rocky scarps are situated in the northern slope of the range, close to the cave. The cave entrance is located in the uppermost part of the higher and older head scarp. Below the minor scarp, a colluvial toe developed at the slope foot (Fig. 3; Margielewski and Urban, 2003a, 2005). The strata orientation and character of gravitational displacement suggest a rotational type of landslides (*sensu* Dikau et al., 1996).

The DIC is composed of several vertical and subvertical widened cracks predisposed mainly by the D_2 joint set (45–55°), situated close to each other in a narrow tension zone subparallel to the ridge axis. The formation of this zone was caused by the shift of the northern slope of the range towards the north and its slight throw (5–25 cm). However, the particular cracks were widened due to various types of movement: translation, slight toppling and rotation. The movement of rigid sandstone blocks was probably facilitated by sliding along a shale insert situated close to the level of the hill foot (Fig. 3; Margielewski and Urban, 2003a, 2005).

The cave galleries are usually high (about 10 m and more) and narrow (0.5-2 m) and arranged in three levels separated by rock blocks trapped in the cracks (Pulina, 1997b). The cave is 365 m long and 42.5 m deep (Klassek and Mleczek, 2009); therefore, it is the deepest cave in the Polish part of the Beskidy Mts considering its real depth under the ground surface.

2.3. Jaskinia Miecharska cave

The Jaskinia Miecharska cave (MIC) is situated in the Beskid Śląski Mts, namely in the right, northern slope of the Malinka creek valley deeply incised into the massif of Mt Malinowska Skała (1152 m a.s.l), about 1.5 km southeast of the MAC (Fig. 1). The slope is formed by the Upper Godula beds of the Silesian Unit (Burtan et al., 1956; Burtan, 1973; Ryłko and Paul, 1992). In this part, the beds are composed of thick-bedded sandstones interbedded with shales (Fig. 4). In this site, the Upper Godula beds belong to the southern flank of the Szczyrk Anticline. The rock strata strike N 260–290°, and dip 12–20° (Burtan et al., 1956; Burtan, 1973; Margielewski et al., 2007), and in this way they are practically parallel to the slope dipping. The rocks are cut by a joint system corresponding to regional master joint sets. The set of longitudinal joints (L) oriented ca. 260–280° and two sets of complementary diagonal joints D_1 = 130–140° and D_2 = 220–240° are well developed, while the set of transversal joints: T = ca. 340° is less distinctly marked (Margielewski et al., 2007).

The MIC is an element of a large landslide covering ca 6 ha of a slope directly above the valley bottom between two tributaries of Malinka creek (Fig. 4A). The landslide represents a complex type (*sensu*; WP/WLI, 1990, 1993; Dikau et al., 1996) combining various types of displacement such as translation (spreading), toppling and rotation which developed during several stages of mass movement (Fig. 4A, L1–L7 stages). From the geomechanic point of view, it represents an intermediate and locally shallow type (*sensu*; Hutchinson, 1995: maximum depth of slip surface located 10–30 m below ground surface) of a gravitational slide. The entrance of the cave is located in a trench at the foot of a secondary scarp of the transformed landslide body (Fig. 4; Margielewski et al., 2007).

The MIC is 1810 m long and its depth under the (inclined) ground is 10–20 m. The cave is composed of a maze system of galleries and chambers which are 0.5–10 m high and 0.3–8 m wide and follow the orientation of the most prominent joint sets: diagonal D_1 and D_2 and transversal T. The cave system is divided into three parts differing in the location within the landslide and predominant direction of cave galleries (Fig. 4). The whole cave system dips to the southwest at an angle of ca. 15° (Fig. 4) and it is almost parallel to the ground surface and strata inclination. In many places, its bottom is identical to the landslide slip surface or it is situated very close to it (Fig. 4B). It is evidenced by the occurrence of a cave stream penetrating as deep as this surface location (but not deeper into non-disintegrated massif; Margielewski et al., 2007). Apart from the MIC, 16 small caves have been identified in the landslide zone. Their length varies from 3 to 34 m, and most of them represent single and simple galleries–widened fractures. Two of the caves represent more complex systems of chambers and passages.

The MIC was formed due to fissure macrodilatancy controlled by joints and bedding (Kranz and Scholz, 1977; Margielewski et al., 2007). It means that during the main stage of mass movement, the block-type displacement was accompanied by the increase in the bulk volume of the massif. Although the initial displacement was controlled by the widening of joints, it was subsequently accompanied by the development of folds in shale inserts as well as brecciation of shales and sandstones produced by brittle destruction in the sliding zone. These types of deformations, characteristic of fissure macrodilatancy, favoured differentiated gravitational displacement within the main landslide body such as rotation around horizontal and vertical axes (Margielewski et al., 2007, 2008).

3. Methods

3.1. Mapping and geomorphological study of the study areas

The caves in the studied areas were found and explored in different time. The MAC and DIC caves have been known since the 19th century, whereas the MIC cave was discovered and explored in 2004. Current maps and descriptions of the two first caves (used in this paper) were published in the inventory of caves of the Outer Carpathians (Ganszer, 1997, Ganszer and Mleczek, 1997; Klassek, 1997a,b; Rachwaniec, 1997). The caves were mapped using a measuring tape and a geological compass. The data of the MIC cave, firstly published by Szura (2006), have continuously been updated up to now (Margielewski et al., 2008; Klassek and Mleczek, 2009). The cave was mapped using a measuring tape, a ranging laser and a geological compass. The classification of caves used in this paper is based on the proposal of Vítek (1983).

A geological and geomorphological study of the MAC and its surroundings (reconstruction of slope evolution) was conducted by Margielewski and Urban (2003a). The map of its surroundings has recently been updated by the authors. Geological and geomorphological description of the DIC and related landforms was published by Margielewski and Urban (2005). Results of the geomorphological study of the MIC and the surrounding landslide were presented by Margielewski et al. (2007); however, the landslide map has recently been supplemented on the basis of data obtained by geodetic and GPS methods.

In order to describe and classify mass movement, we used a typology according to the International Geotechnical Societes' UNESCO Working Party on World Landslide Inventory (WP/WLI, 1990, 1993; Dikau et al., 1996; Turner and Schuster, 1996). The

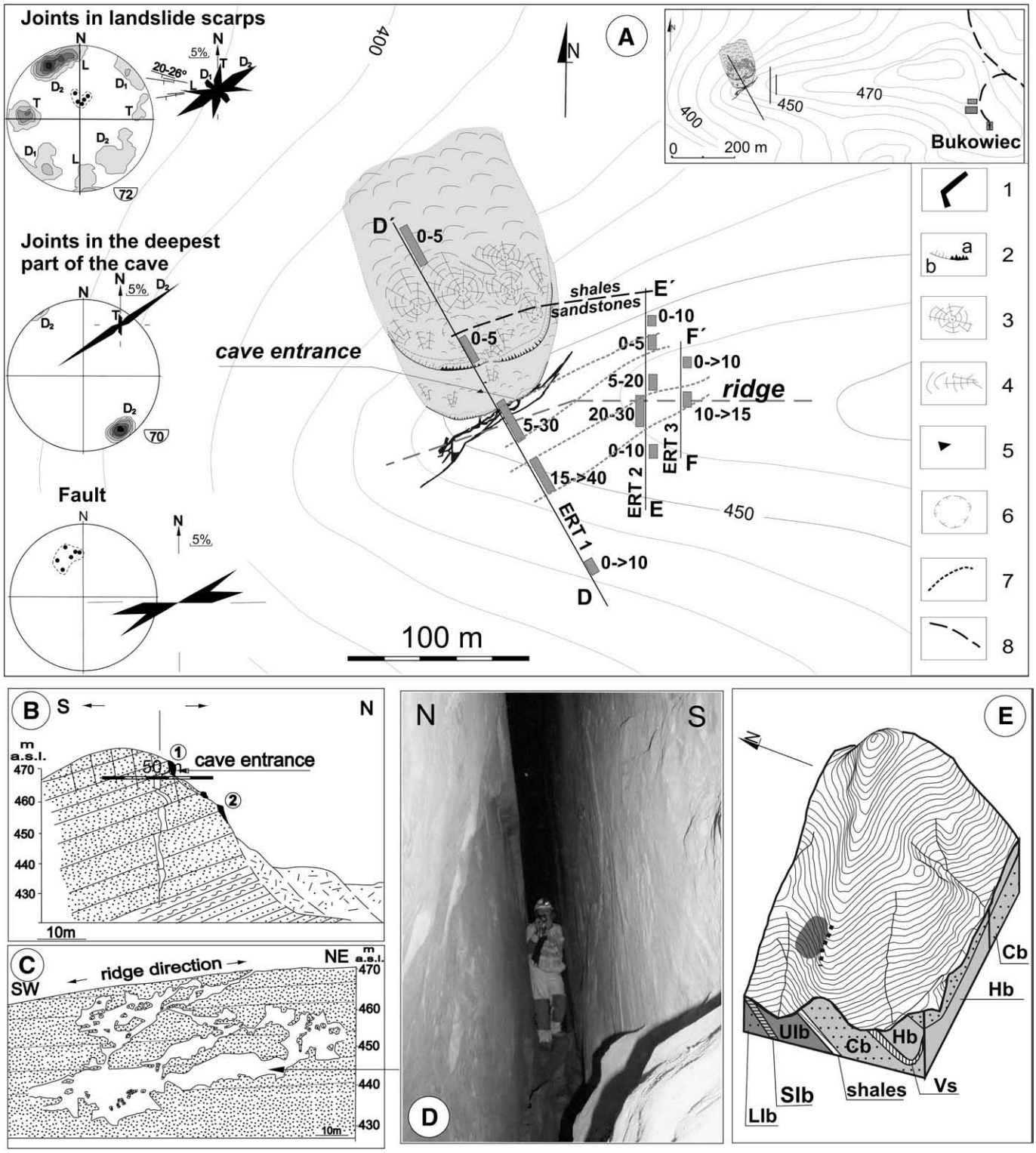

Fig. 3. Diabla Dziura Cave site. (A) A map of the cave (simplified after Ganszer and Mleczek 1997) and its surroundings as well as rose, contour and pole point diagrams. Explanation of symbols in the legend: 1—cave; 2—scarp: a—rocky, b—soil; 3—landslide body (ramparts); 4—creeping and colluvial tongue; 5—rock forms; 6—depression; 7—probable contour (outcrop) of high-resistivity bodies; 8—probable outcrop of shale–sandstone boundary inferred from the ERT; other symbols—see Fig. 2; steeply dipping ERT profiles are shortened according to their projection on horizontal plane. Bedding planes in the pole point diagram. Fault plane in rose and pole point diagrams (explanation for the diagrams in Fig. 2). (B) Conceptual model of the transversal cross section of the cave and geological structure (after Margielewski and Urban, 2003b). (C) Longitudinal cross section of the cave (simplified after Ganszer and Mleczek, 1997). (D) Photo of one of the typical gallery in the deepest part of the cave. (E) Orthogonal projection of Mt Bukowiec with location of the Diabla Dziura Cave (dotted line) and a landslide (dark grey) and geological cross sections: Llb—Lower Istebna beds; Slb—shales of Istebna Beds; Ulb—Upper Istebna beds; Cb—Ciężkowice beds; Vs—Palaeocene shales; Hb—Hieroglyphic beds (after Margielewski and Urban, 2003b).

description of joint system used in the analysis of caves corresponds to the proposals of Mastella et al. (1997).

3.2. Application of ERT

The application of resistivity methods in geology and geomorphology is based on an assumption that various entities like minerals, solid bedrock, sediments, air and water differ in electrical conductivity/resistivity (Milsom, 2005; Kneisel, 2006; Schrott and Sass, 2008). In our case, we suppose strong geoelectrical contrasts between bedrock and air-filled subsurface voids like widened fractures (caves) or zones formed by systems of closely spaced crevices. Additional contrasting subsurface objects assumed in the studied slope deformations are shear/slip zones, lithological and tectonic boundaries, surficial scree deposits, water table and perched aquifers.

The principle of ERT sounding consists in the application of constant direct current into the ground via two current electrodes and measuring the resulting voltage at two potential electrodes. The method is based on multielectrode and multicabel system; each of the electrodes alternatively acts as a current and potential electrode and the whole profile is measured without the intervention of surveyors. The position of current and potential electrodes during the measurement is dependent on the chosen geometry of electrode arrays (Fig. 5). Most frequently used arrays are the dipole–dipole, Wenner and Wenner–Schlumberger arrays (e.g. Milsom, 2005; Kneisel, 2006; Schrott and Sass, 2008; Fazzito et al., 2009). The dipole–dipole method uses two current electrodes on one side and two potential on the other side. The method is especially suitable for the detection of vertical structures as it penetrates to deeper levels (Candansayar, 2008). Main disadvantages are sensitivity to high near-surface resistivity and time consumption (Szalai and Szarka, 2008a). The Wenner array comprises four equally spaced electrodes deployed in a line in which potential electrodes are situated between current electrodes. Main advantage of the method is high resolution of horizontal heterogeneities, stability, low sensitivity and comparatively short survey (total number of measured points is lower than in dipole–dipole). Disadvantages comprise shallower penetration and less subsurface information in comparison with the dipole–dipole array (Szalai et al., 2009). The Wenner–Schlumberger configuration is similar to the Wenner array; potential electrode spacing is constant but current electrode spacing is logarithmically increased. The method is a compromise between the dipole–dipole and the Wenner arrays as it assures quite deep penetration, reliable stability and ability to detect both horizontal and vertical subsurface structures.

Data obtained during field ERT measurements are classically presented as apparent resistivity pseudo-sections, which give an approximate picture of the subsurface resistivity. To obtain a true model representing continuous distribution of calculated electrical resistivity in the subsurface, inversion procedure is utilized (Loke and Barker, 1996). The difference between measured apparent resistivity values and inverted results is expressed by a root-mean-squared (RMS) error (Loke, 1997; Milsom, 2005). The value of the RMS error is one of the important factors in the selection of the best appropriate electrode array (Kneisel, 2006).

We measured 14 ERT profiles including three sections at the MAC site, three sections at the DIC site and eight sections at the MIC site. Technical parameters of sounding are described in Table 1. The majority of profiles were measured by at least two contrasting techniques—usually the dipole–dipole and the Wenner arrays. The main localization strategy was (i) to select profiles across well-mapped subsurface structures with the aim to obtain typical resistivity evidence and (ii) to situate additional profiles through sites with similar morphological expression but unknown caves. Similar geoelectrical evidence then helped to extrapolate known structures to the zones with the lack of speleological discoveries. The dipole–dipole electrode array was chosen as a key for further interpretations as it gave a reliable RMS error and good description of mapped structures (Table 1). The ability of the dipole–dipole array was enhanced by the fact that the entire measurement was carried out in an abnormally wet period (June 2009) when the topsoil was saturated by water which favoured penetration and quality of signal. The sounding was technically realized by means of a multielectrode system of 64 electrodes connected to an ARES georesistivimeter. Longer profiles were performed by a roll-along acquisition technique. Used electrode spacing varied between 1 and 5 m in accordance with the required resolution and the depth of a particular measured section. The inversion of measured apparent resistivities was provided using the RES2DINV software (Loke and Barker, 1996).

4. Results

4.1. Geoelectrical evidence of crevices (caves) and other gravitational structures of slopes

This chapter provides the description of main geoelectrical evidence of known crevice-type caves in three case localities. Besides the analysis of known structures, we propose to perform their possible ERT-derived continuations and to outline the connection with geoelectrically identified lithological, tectonic and slope deformation elements. All interpretations are made using the dipole–dipole electrode arrays.

4.1.1. Case study: Jaskinia Malinowska Cave (MAC)

Due to its generally narrow passages (0.5–2 m), the presence of the MAC is less clearly detected using arrays with a 3-m electrode spacing. Known cave passages (A–A′ and B–B′ sections) reveal resistivities >1500–2000 Ω m (Fig. 6). The resistivity record of A–A′ profile shows a relatively weak subvertical signal of the longest passage related to the widened D_1 joint system (anomaly A; Fig. 6). High-resistivity anomaly (~1600 Ω m) situated at a depth of 20–30 m (below the longest cave passage) indicates possible deeper continuation of widened crevices. Another highly possible crevice zone (>4000 Ω m; anomaly B) is between ca. 115–135 m on the A–A′ at a depth of 15–25 m. This downslope-elongated high-resistivity zone may indicate widened crevices connected with the evolution of shear zone of future impending landslide (Figs. 2 and 6).

The contour-parallel B–B′ profile reveals two branches of known cave passages in different ways. While the eastern branch of the cave (widened joints of D_2 set) has a rather weak geoelectrical signal, the western branch predisposed by other D_2 joints is displayed much better with a contrasting zone >2000 Ω m (Fig. 6). It is most probably caused by a different shape of the branches—the eastern passage is narrow, formed between blocks, whereas the western passage is several meters high and 0.5–1 m wide (Fig. 2, photo). Pronounced westward continuation of this zone indicates widened crevices at a depth of 10–15 m (Fig. 6, 135–145 m of B–B′), unexplored by cavers yet. This high-resistivity anomaly is spatially connected with the sinkholes situated 10–15 m upslope the B–B′ profile (Fig. 2). Low-resistivity zone (<200 Ω m) in the deepest parts (>20–30 m) of the A–A′ and B–B′ profiles probably corresponds with undisturbed

Fig. 4. Jaskinia Miecharska Cave site (after Margielewski et al., 2007). (A) A map of landslide and the cave. L1–L7—stages of landslide development transforming the landslide zone; steeply dipping ERT profiles are shortened according to their projection on the horizontal plane. Rose and contour diagrams of joint systems in situ rocks measured in the valley bottom of the Malinka creek. (B) Cross section with the orientation of bedding planes (cave's bottom) in contour diagrams (equal area plot—explanations on Fig. 2). Photos of the elements of the cave pointed out with arrows. Explanation of symbols: 1—cave; 2—rock forms: a—crags and rock packets, b—rock block and debris; 3—rocks in cross section: a—landslide body, b—shale and sandstone of bedrock (in situ); 4—spring; 5—ERT profile with marked high-resistivity anomalies: a—apparent high-resistivity signal and its depth in meters, b—less apparent high-resistivity signal and its depth in meters. For other explanations see Figs. 2 and 3.

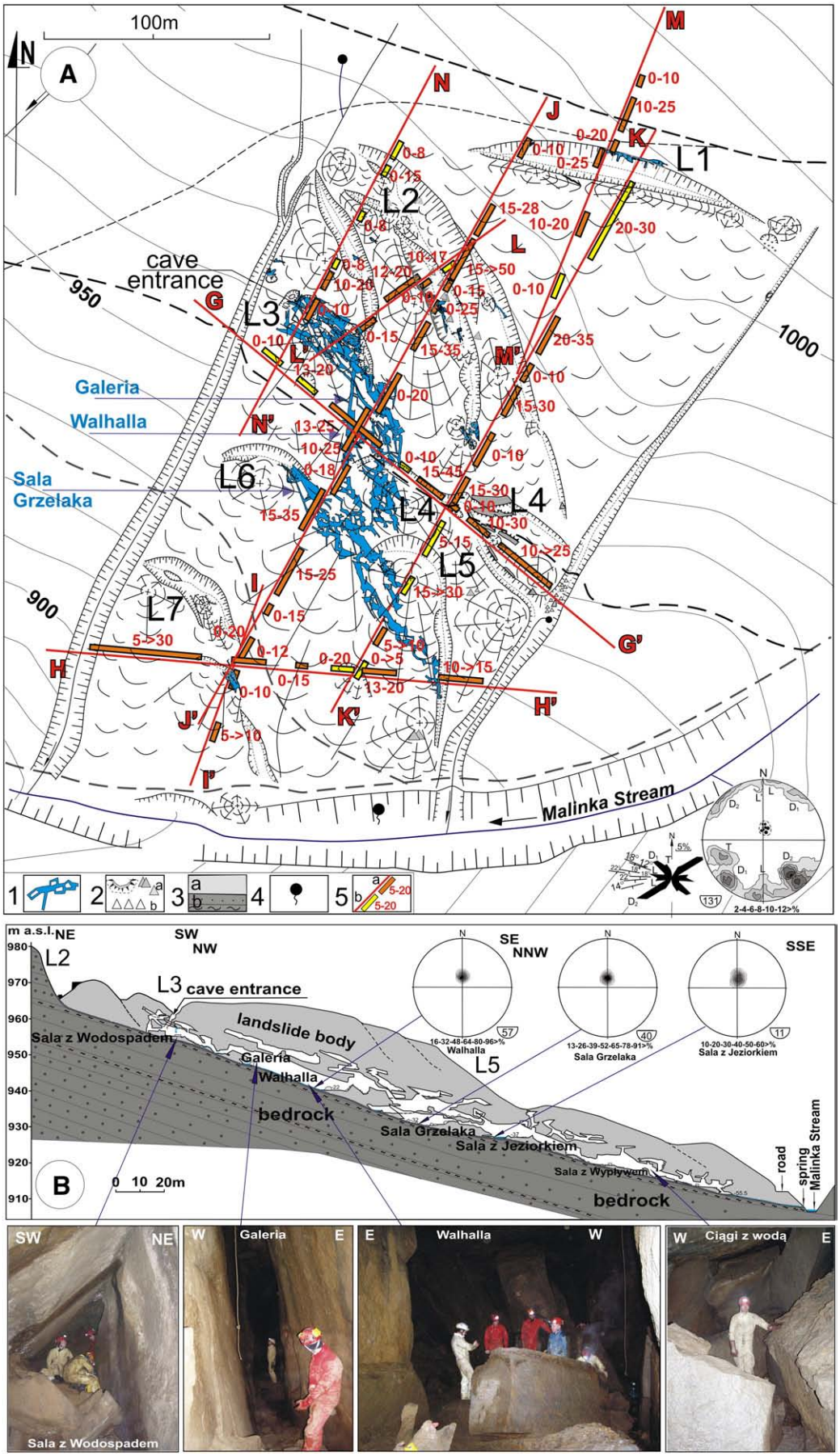
100m
N
A
cave entrance
Galeria
Walhalla
Sala Grzelaka
Malinka Stream
950
1000
900
L1
L2
L3
L4
L5
L6
L7
G
G'
H
H'
I
I'
J'
K'
L'
M'
N'
1
2
3
4
5
m a.s.l.
NE
SW
NW
SE
NNW
SSE
L2
L3 cave entrance
landslide body
Sala z Wodospadem
Galeria
Walhalla
bedrock
Sala Grzelaka
Sala z Jeziorkiem
Sala z Wypływem
road
spring
Malinka Stream
B
0 10 20m
16-32-48-64-80-96>%
13-26-39-52-65-78-91>%
10-20-30-40-50-60>%
2-4-6-8-10-12>%
SW
NE
W
Galeria
E
E
Walhalla
W
W
Ciągi z wodą
E
Sala z Wodospadem

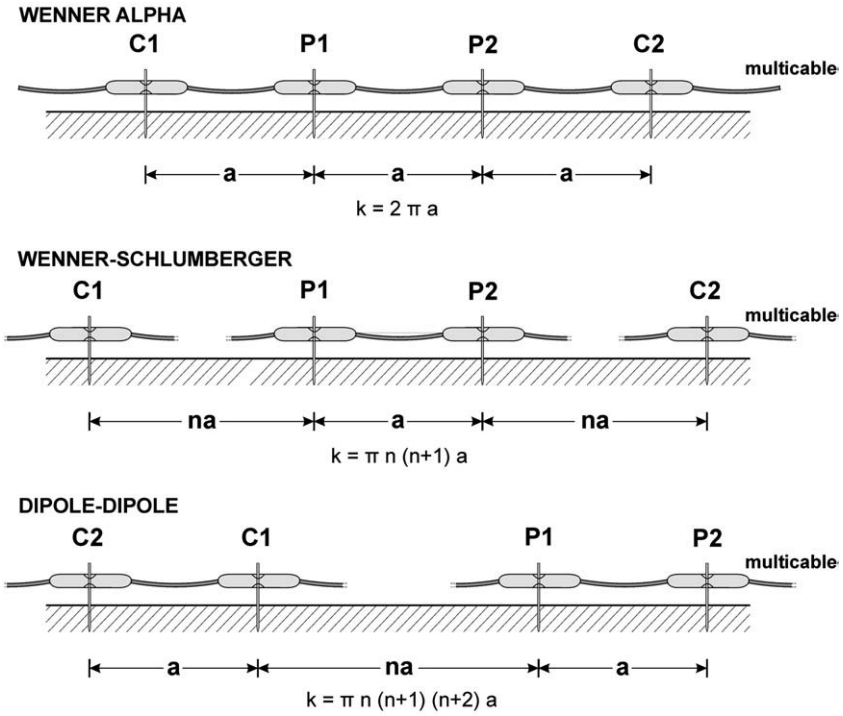

Fig. 5. Electrode arrangement for different arrays. Explanation of indexes: C1,2—current electrodes; P1,2—potential (measuring) electrodes; k—geometric factor; a—distance between the electrodes (after Loke, 1997).

bedrock situated below the fractured zone affected by mass movement activity.

Possible westward continuation of crevice-type caves at the MAC site was detected by the C-C′ profile (with a 2-m electrode spacing) situated across expected prolongation of the MAC (Fig. 6). The most striking evidence of a widened and less than a 10-m-deep crevice-type element (>8000 Ω m) is identified above a sinkhole situated at 60–64 m from the north beginning of the section. This structure lies in the western prolongation of anomaly A (the longest cave passage) and reveals a likely continuation of widened (D_1-related) crevices. Other possible widened crevices are situated in deeper parts of the profile (10–20 m) just under the sinkhole. The first structure (anomaly D) situated at ca. 60–70 m may indicate incipient headscarp of a future landslide. Another high-resistivity anomaly at 88–92 m lies directly in the continuation of the western branch of the MAC (anomaly C) and possibly presents D_2-related widened crevices (Figs. 2 and 6).

Table 1
Summary of technical parameters of ERT measurement.

Parameter	Value
Total length of profiles	2683 m
Number of profiles	14
Number of dipole–dipole profiles	14
Number of Wenner profiles	9
Number of Wenner Schlumberger profiles	5
Longest profile	355 m
Shortest profile	63 m
Average RMS error for dipole dipole profiles	10.9%
Average RMS error for Wenner profiles	4.6%
Average RMS error for Wenner Schlumberger profiles	6.6%
Average measured points per section	1159
Maximum measured points per section	1971
Minimum measured points per section	359
Approximate average penetrating depth of profiles*	39
Approximate maximum penetrating depth of profiles*	65
Approximate minimum penetrating depth of profiles*	16
Period of measurements	June 2—30, 2009

*Measured in central (deepest) parts of dipole–dipole profiles.

4.1.2. Case study: Jaskinia Diabla Dziura Cave (DIC)

The D–D′ profile displays overall tectonic, lithological and slope deformation features of the investigated ridge. The first-order pattern of the geoelectrical structure is given by the presence of two high-resistivity (>500 Ω m) bodies of massive Ciężkowice sandstone. One of them is situated in the uppermost part of the hill ridge and overlies low-resistive (<50 Ω m) shale series (Fig. 7). The other body is situated much deeper within the southern slope, below the level of relative low-resistivity, which points to the presence of sandstone–shale series. It indicates tectonic vertical displacement of southern and northern entities and discontinuity between them; however, the spatial orientation of the fault can be similar to the orientation of joints (shown in upper two diagrams of Fig. 3A) or to the fault plane found in the cave (lower diagram of Fig. 3A).

The presence of explored DIC is well detected by the D–D′ profile but the corresponding high-resistivity zone (>5000 Ω m) is shifted slightly southward and it is much wider than the speleologically investigated cave system (Figs. 3 and 7). This record may indicate that the number of unexplored widened crevices (related to D_2 joint set) is higher in the upper relaxed part of the rock massif (Fig. 7, depth 10–25 m, anomaly A), if compared with deeper levels where single narrow passages predominate. The deepest cave passages (at a depth of at least 30 m) are only weakly detected in the D–D′ profile electrical image. The most probable explanation is their possible immediate ending at the upper surface of shale series marked by low resistive body on the profile. A possible zone of widened crevices likely predisposed by D_2 joint set is situated within the deeper sandstone body at ca. 68–88 m from the south beginning of the D–D′ profile (i.e. ~35 m southeastward from the DIC) at a depth below 15 m (Fig. 7, anomaly B). Internal resistivity variations within the sandstone body are determined, besides crevice zones, also by shear surface of an old rotational landslide situated on the northern slope of the ridge (Figs. 3 and 7). Distinct resistivity record exhibits a ~10-m-thick landslide

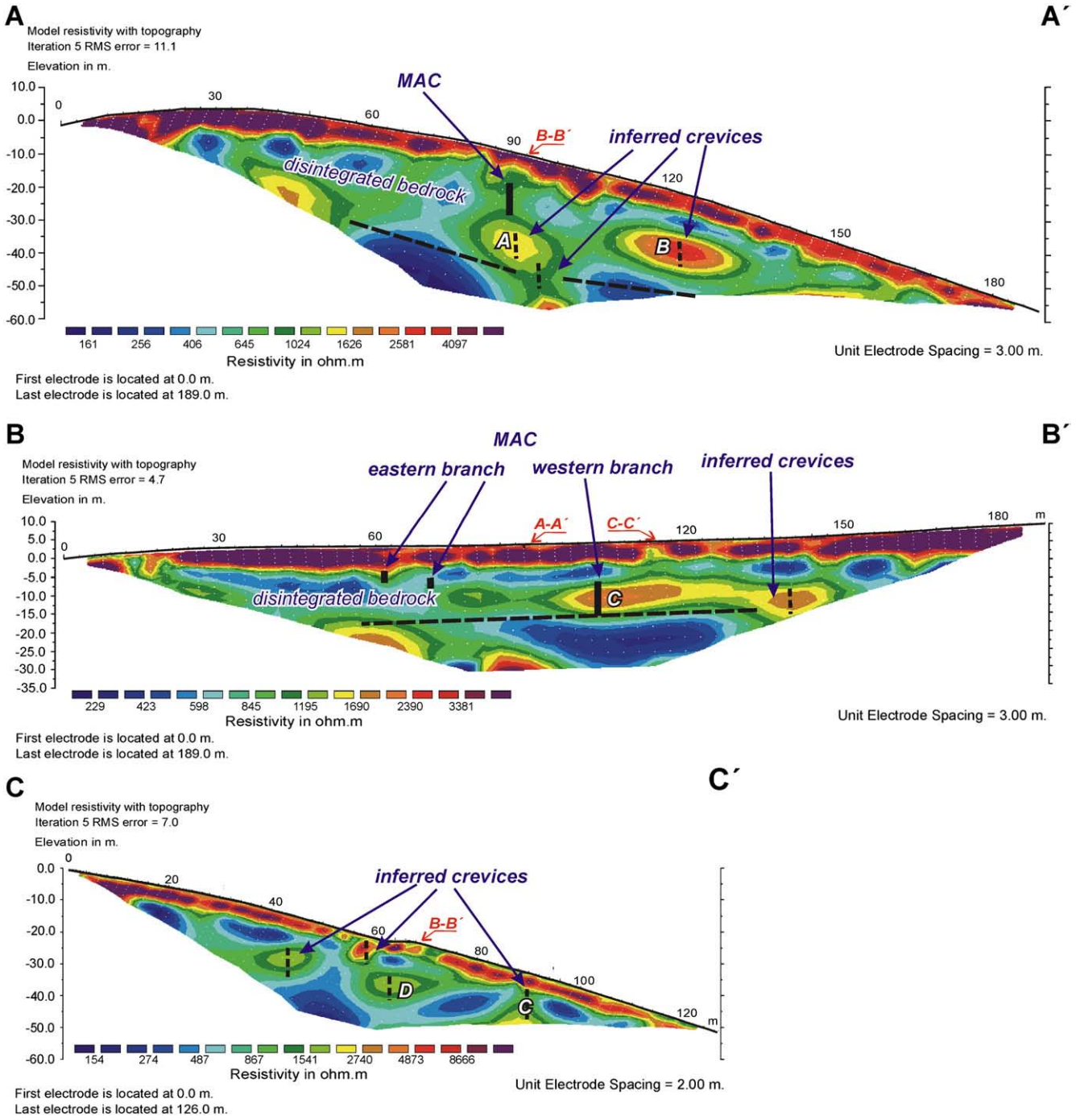

Fig. 6. Resistivity tomograms of dipole–dipole surveys in the MAC site (for profile localization see Fig. 2). High-resistivity zones situated in the deepest parts of the profiles were not interpreted and can be considered artifacts that resulted due to inversion procedure.

colluvium overlying low-resistivity shales at ca. 184–252 m of the D–D′ profile.

The existence of possible widened crevices situated northeast of the DIC was checked by two shorter, high-resolution profiles using a 2- and 1-m electrode spacing (Figs. 3 and 7). Both the E–E′ and F–F′ profiles display a shallow subvertical high-resistivity zone (ca. 2000 Ω m) situated north off the ridgeline, which can be correlated with anomaly A on the D–D′ profile and interpreted as an array of fractures that is a continuation of the Diabla Dziura fissure zone. The apparent high-resistivity deep-seated body in the E–E′ profile refers also to anomaly B in the D–D′ profile. This anomaly is less apparent in the F–F′ profile probably due to shallow vertical extension of this profile.

4.1.3. Case study: Jaskinia Miecharska Cave (MIC)

The total of eight ERT sections were surveyed in the MIC site including four long profiles with a 5-m electrode spacing (two longitudinal and two transversal sections crossing the entire landslide body) and four additional sections of shorter electrode spacing and higher resolution (Fig. 4). Longer and deeper penetrating profiles (G–G′, H–H′, J–J′, K–K′, M–M′ and N–N′) reveal ca. 20–30-m-thick subsurface zone with numerous high-resistivity wedges and lenses overlying a more conductive (<300 Ω m) sector (with a different pattern of scarce high-resistivity entities). These detected resistivity anomalies usually pass between individual profiles (see letters A–I marked in Fig. 8). We interpret high-resistivity anomaly as the concentration of fractures or other voids. The underlying conductive

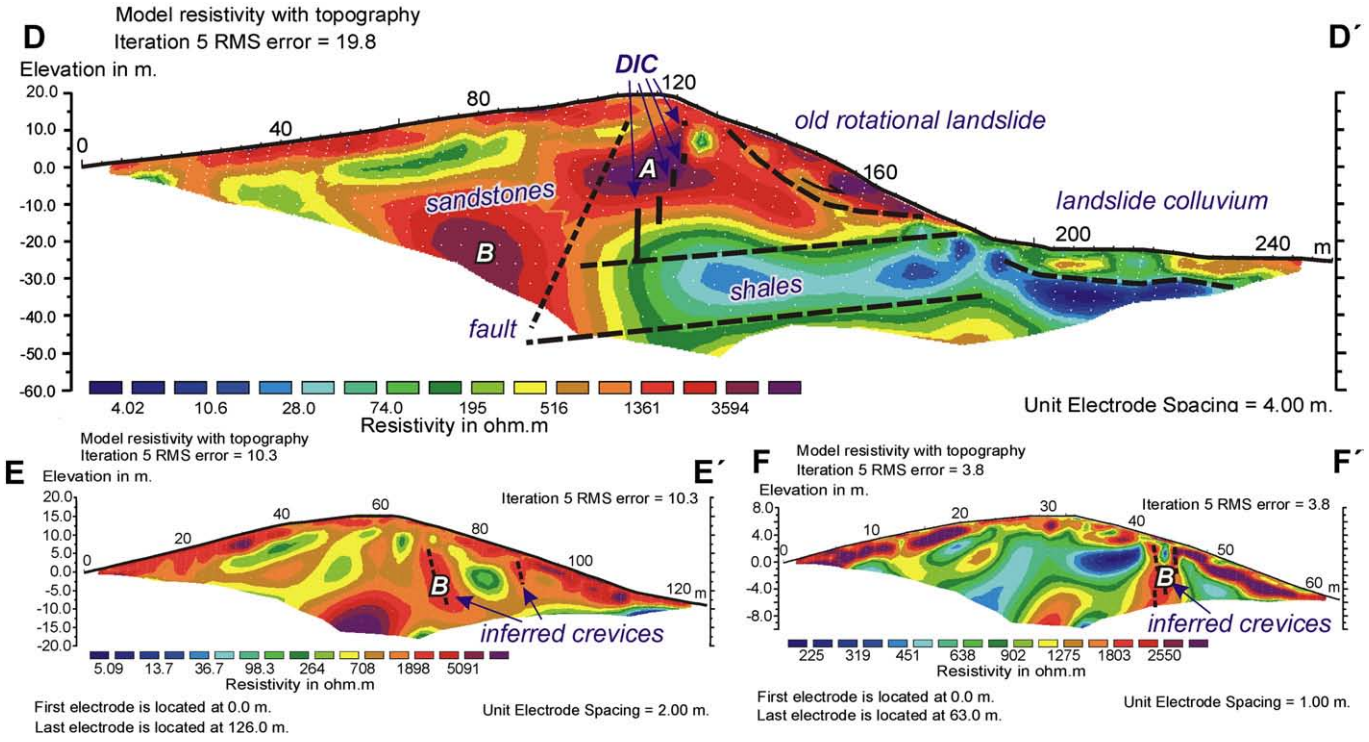

Fig. 7. Resistivity tomograms of dipole–dipole surveys in the DIC site (for profile localization see Fig. 3).

zone reflects most likely undisturbed bedrock; the transition zone between both contrasting resistivity bodies can thus be interpreted as slip (shear) surface (Fig. 8). Some of high-resistivity anomalies almost interrupt the underlying conductive zone (G–G′, H–H′, I–I′ and J–J′ profiles) indicating fissure-related passages just on the shear surface.

The ERT sounding detected well-speleologically explored cave chambers as high-resistivity zones with >2000–3000 Ω m. It especially applies to the Walhalla chamber (15 m long, 8 m wide and 8 m high), Grzelak's chamber and high Galeria passage situated in the vicinity of Walhalla (Fig. 4). These passages and chambers are well reflected even with a 5-m electrode spacing (see G–G′ and J–J′ in Fig. 8). Walhalla chamber is excellently detected in both longitudinal (J–J′) and transversal (G–G′) sections. It must be emphasized that the location of this chamber just on the slip surface confirms the above interpretation of the transition zone between bodies of a contrasting resistivity pattern.

Besides detected known cave passages, numerous subvertical zones of a depth of up to 20 m and resistivities exceeding 2000–3000 Ω m (some of them even >10 000 Ω m) are identified on the basis of the presence of scarps and trenches as shown in Fig. 4 as L1–L7. Investigated structures are usually identical or adjacent to newly explored minor caves situated around the main MIC (Fig. 4). These caves are numerous phenomena connected with local relaxation of rock mass and widening of T and D_1, less frequently L joint sets in steepened parts of the slope at the main scarps (e.g. anomaly A in J–J′ and L–L′ profiles) or minor scarps (e.g. anomaly C in J–J′ and L–L′ profiles). Detected anomalies below L1 and L7 (anomalies F and I) indicate rather localized subvertical (but well depicted) D_1 or L-related crevices up to 10–20 m deep. Particularly pronounced anomaly F is situated below the sinkhole in the lowermost part of the landslide. This subvertical structure was verified by three profiles (H–H′, I–I′, J–J′) using various electrode spacing (Fig. 8). Potential laterally extensive crevice-type caves or systems of inaccessible crevices are found in wider surrounding of L2 trench, just above the upper part of the MIC. Both subvertical crevices (i.e. anomaly B related to widened D_1 joint system) and laterally prolonged, shear zone-parallel crevices (i.e. anomaly D) can be expected in this zone. Possible eastward continuation of the MIC (just eastward from Walhalla) is detected around L4 scarp/trench at a depth of ca. 20 m (Fig. 4).

4.2. Displaying of gravitationally induced cavities using various electrode arrays and spacing

A majority of performed profiles were measured by at least two different electrode arrays in order to test the reliability of contrasting geoelectrical techniques. Typical examples of various results obtained by the comparison of the dipole–dipole, Wenner–Schlumberger and Wenner arrays are presented in this chapter (Fig. 9). Our data indicate that the application of an appropriate electrode array seems to be crucial in the investigation of cavities and in the determination of their approximate geometry and subsurface position.

If we compare individual electrode arrays, some sections (e.g. G–G′ profile with Walhalla; Fig. 9A) reveal great differences in cave detection. While the dipole–dipole arrays fit the mapped cave elements very well, other techniques (less sensitive to lateral heterogeneities) rather fail to detect the position of known structures. The resulting tomography displays only generalized geometry and the location of structures is both laterally and vertically shifted (see e.g. the Walhalla chamber in Fig. 9A). It holds good for the investigation of pronounced cave chambers and passages. When applied to less significant (narrow) passages (like the MAC; Fig. 9B), which are only poorly detected by the dipole–dipole array, the resulting tomography performed by the Wenner technique is even worse and shows no signal of the existing cave system. On the contrary, in case we focus on

Fig. 8. Resistivity tomograms of dipole–dipole surveys in the MIC site (for profile localization see Fig. 4). High-resistivity zones situated in the deepest parts of the profiles were not interpreted and can be considered artifacts that resulted due to inversion procedure.

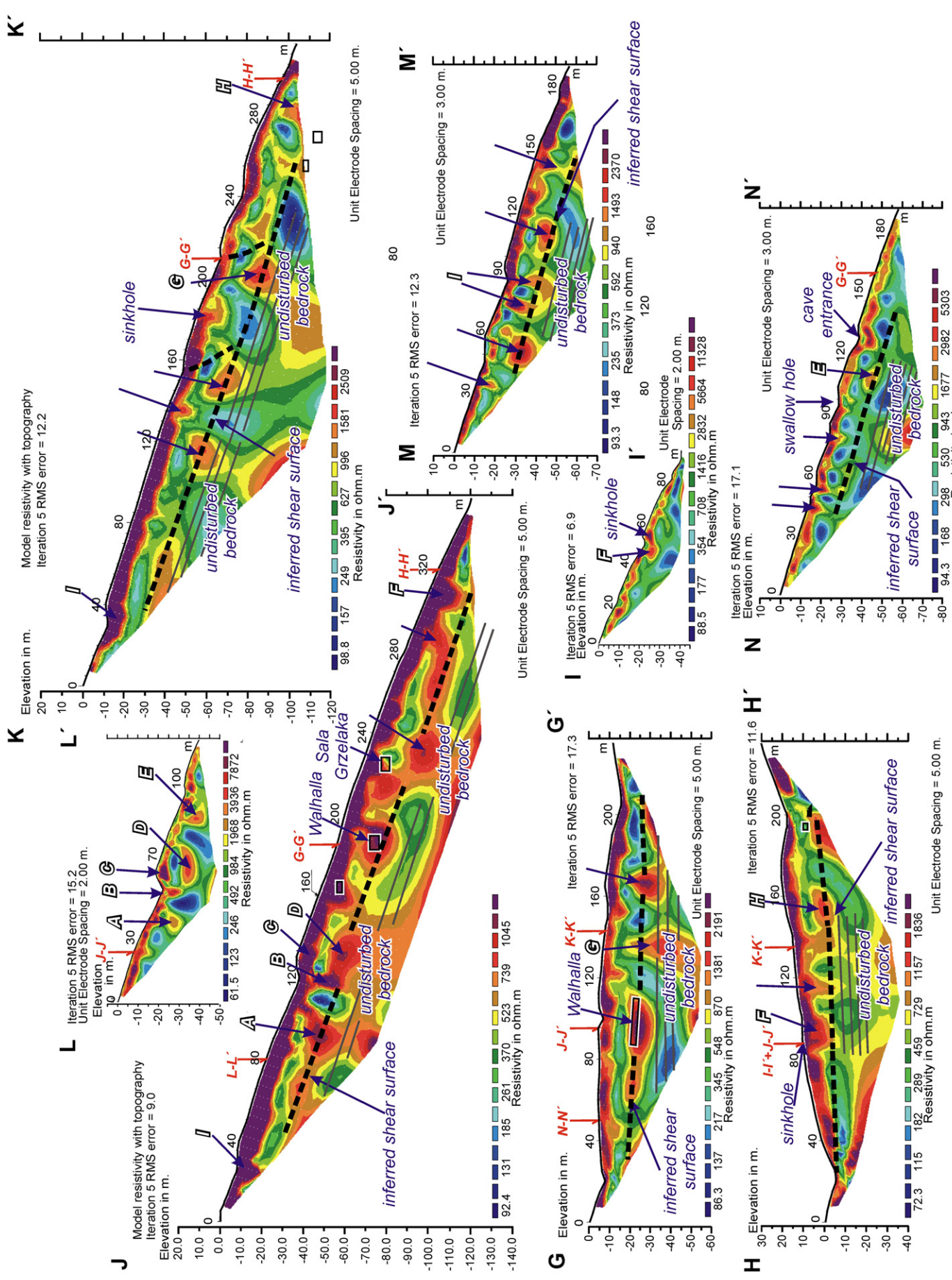
K´
K
Model resistivity with topography
Iteration 5 RMS error = 12.2
Elevation in m.
sinkhole
undisturbed bedrock
inferred shear surface
Unit Electrode Spacing = 5.00 m.
Resistivity in ohm.m
L´
L
Iteration 5 RMS error = 15.2
Unit Electrode Spacing = 2.00 m.
Elevation J-J´ in m.
Resistivity in ohm.m
J´
J
Model resistivity with topography
Iteration 5 RMS error = 9.0
Elevation in m.
Walhalla Sala Grzelaka
undisturbed bedrock
inferred shear surface
Unit Electrode Spacing = 5.00 m.
Resistivity in ohm.m
M´
M
Iteration 5 RMS error = 12.3
Unit Electrode Spacing = 3.00 m.
undisturbed bedrock
I´
I
Iteration 5 RMS error = 6.9
Elevation in m.
sinkhole
Unit Electrode Spacing = 2.00 m.
Resistivity in ohm.m
inferred shear surface
N´
N
Iteration 5 RMS error = 17.1
Elevation in m.
swallow hole
cave entrance
inferred shear surface
undisturbed bedrock
Unit Electrode Spacing = 3.00 m.
Resistivity in ohm.m
G´
G
Iteration 5 RMS error = 17.3
Elevation in m.
Walhalla
inferred shear surface
undisturbed bedrock
Unit Electrode Spacing = 5.00 m.
Resistivity in ohm.m
H´
H
Iteration 5 RMS error = 11.6
Elevation in m.
sinkhole
undisturbed bedrock
inferred shear surface
Unit Electrode Spacing = 5.00 m.

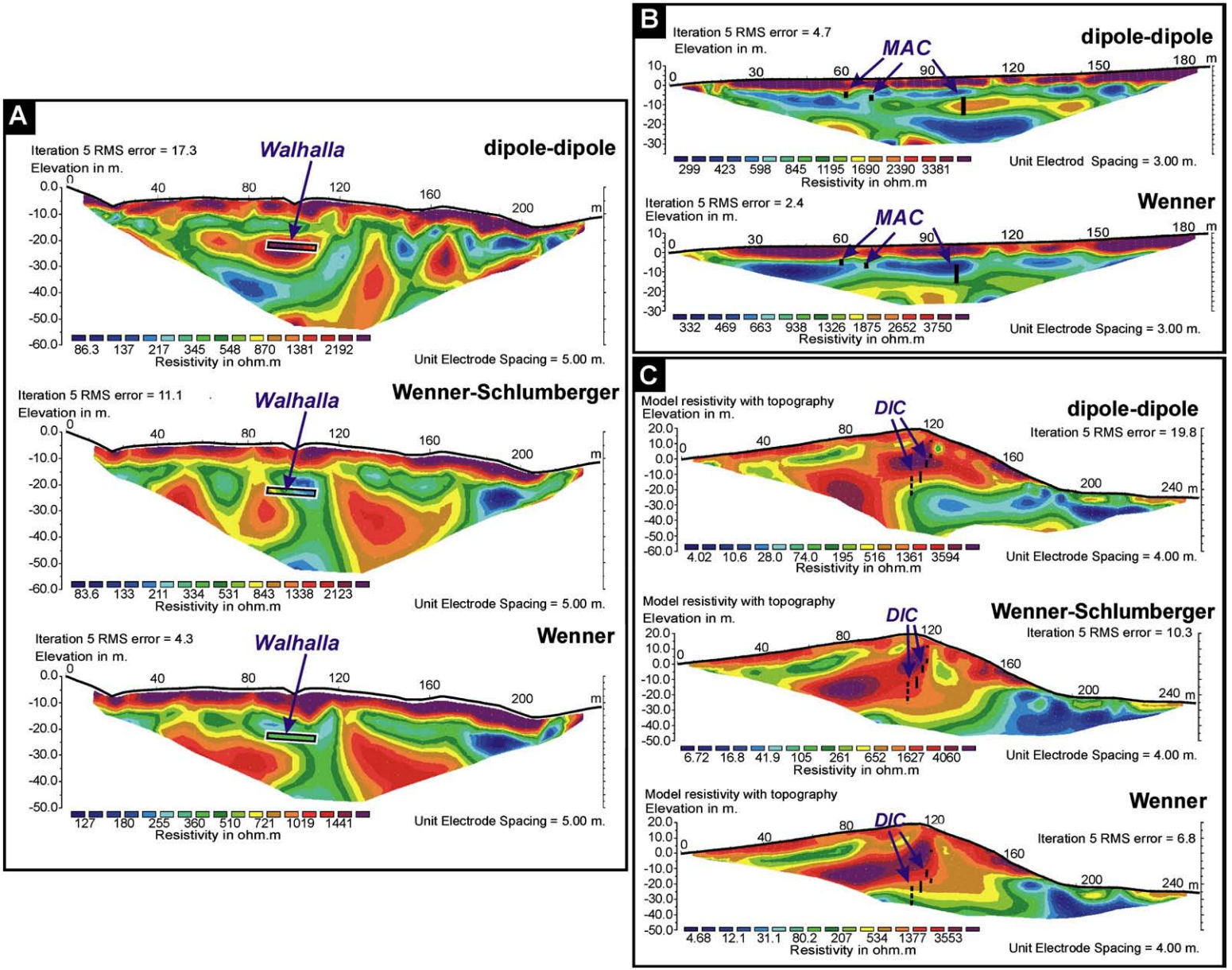

Fig. 9. Comparison of the reliability of detection of known cave passages using different electrode configurations. (A) Section across the most pronounced chamber (Walhalla) within the MIC site (equivalent to G–G′ in Fig. 8). (B) Section across the MAC site (equivalent to B–B′ in Fig. 6). (C) Section across the DIC site (equivalent to D–D′ in Fig. 7). High-resistivity zones situated in the deepest parts of the profiles were not interpreted and can be considered artifacts that resulted due to inversion procedure.

subsurface structure that is rather distinct and formed by a wider zone of parallel cavities, the tomography results of different electrode arrays converge, as shown in the DIC example (Fig. 9C). Such systems of crevice-type caves are even detected by the Wenner array, although it is considered as the worst technique used in the identification of vertical structures.

Interesting results were obtained by the application of various arrays and different electrode spacing (Fig. 10). It is obvious that shorter electrode spacing assures higher resolution of subsurface structures (e.g. the I–I′, J–J′ and L–L′ profiles in the MIC; Fig. 8). Profiles studied using a 5-m electrode spacing display systems of crevices whereas 2-m spacing sections rather reveal individual crevices. Our research furthermore indicates that in case various electrode arrays are applied, shorter electrode spacing eliminates differences in the ERT record (see the I–I′ and L–L′ profiles of the MIC site studied using a 2-m electrode spacing; Fig. 10). From the viewpoint of the detection of crevices, differences between the dipole–dipole and the Wenner–Schlumberger or the Wenner arrays are then rather negligible. The Wenner array (see the L–L′ section; Fig. 10) displays the same structures (anomalies A, B, C and D) but in slightly deeper levels. Differences between the dipole–dipole and the Wenner–Schlumberger arrays are also small in the case of the I–I′ profile (i.e. anomaly F displayed in Fig. 8) in the MIC site.

5. Discussion

5.1. Methodological remarks

Subsurface cavities of various sizes are contrasting geophysical objects and they usually behave as geoelectrical, seismic and/or gravity anomalies (Abu-Shariah, 2009). The interpretation of resistivity properties should not always be straightforward (Van Schoor,

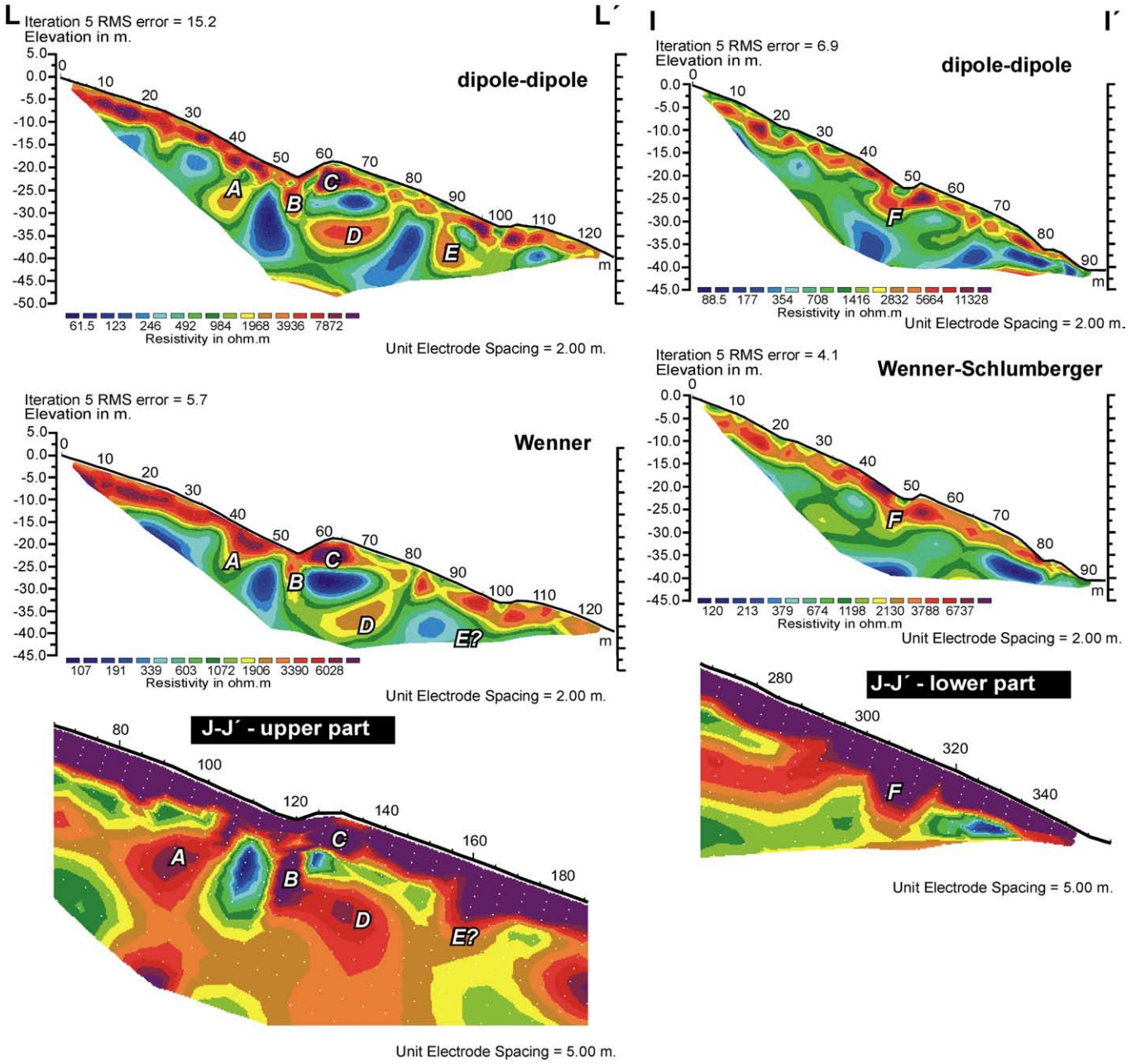

Fig. 10. Effect of electrode spacing and different configurations on the geometry of discontinuities detected by selected profiles within the MIC site.

2002). We must distinguish especially air-filled (high-resistivity) and water-filled (low-resistivity) cavities and fractures (Van Schoor, 2002; Zhou et al., 2002; Abu-Shariah, 2009; Heincke et al., 2010). The latter are abundant in carbonate karst areas and are characterized as pronounced low-resistivity anomalies (Abu-Shariah, 2009). Although some fractures and fracture zones in non-carbonate bedrock are also saturated by water (Heincke et al., 2010), our examples of pseudokarst cavities in sandstone-bearing formations usually show significant high-resistivity anomalies. The performed study shows that the ERT technique is a suitable tool in the detection of crevice-type caves if no other geophysical methods are used. This hold true especially if well-documented known cavities are found in an investigated area and the surveyor is able to obtain a typical record of the investigated caves. In other cases, a combination of at least two geophysical techniques is highly recommended (Schrott and Sass, 2008).

One of the disadvantages of geoelectrical techniques is that each material can be characterized by a relatively wide range of possible resistivities depending on the actual physical and chemical states of rock massifs (Schrott and Sass, 2008; Abu-Shariah, 2009). As some of these parameters are season dependent, the resistivity of a particular object reveals temporal variations. Resistivity values of detected cavities in our study sites vary even within individual localities, for instance detected cavities in the MIC site range between ~1000 and >10 000 Ω m. As shown in other studies (e.g. Ezersky, 2008) pronounced cavities in bedrock with generally higher conductivity (Quaternary deposits) even reveal resistivities of <500 Ω m. These results indicate that subsurface cavities have no typical resistivity values. Besides measurement-related factors, this resistivity parameter is influenced by both internal (geometry and size of caves) and external (physical and chemical composition of the cave's surrounding) conditions.

Another implication of the performed study concerns the geometry of obtained cave-related high-resistivity anomalies. As in the study of Ezersky (2008), anomalies larger than known cave chambers and passages were detected in this study (see e.g. the MIC or DIC sites). Such discrepancy can partly be explained by inversion modeling which displays contrasting but narrow objects such as bowl-shaped structures. Another explanation of such phenomena lies in the character of bedrock and extension of the existing cave systems—we can expect that the mapped crevice-type caves represent only a portion of really existing air-filled cavities. Wider high-resistivity zones surrounding the cavities are also affected by rock/soil decompaction in the vicinity of gravitationally induced caves. Deciphering such problems could be solved in the future by the implementation of other geophysical techniques, the most suitable of which seems to be microgravimetry and ground penetration radar (Beres et al., 2001).

As one of the first ERT studies, our work tried to evaluate various electrode arrays in cave detection directly by numerous field measurements. Based on our data, the choice of reliable arrays is crucial in the detection of air-filled cavities. The dipole–dipole array brought the best results in the detection of known structures and its interpretation seems to be most reliable for the extrapolation of non-investigated areas. This finding is in accordance with similar studies performed in karst environments (Zhou et al., 2000, 2002). The reliability of the dipole–dipole configuration is supported by its best results in cave detection despite a worse signal-to-noise ratio and a higher RMS error, if compared with the Wenner and Wenner–Schlumberger arrays (see Table 1). In accordance with Zhou et al. (2002), our data set indicates that the Wenner array cannot provide recognizable evidence of narrow air-filled cavities and thus its use should be avoided in similar studies (especially in the case of wide electrode spacing). As there are several tens of other possible electrode configurations (Szalai and Szarka, 2008b), other combinations (e.g. pole–dipole) should be tested for the studied problem in the future.

5.2. Implications for the understanding of mass movement in anisotropic flysch massifs

Besides surface landforms, pseudokarst caves are the most important elements studied in order to reconstruct structures of gravitationally transformed slopes. The ERT method expands the possibility of slope structure studies because caves represent only such a part of fractures that is accessible to people (explored by cavers). Also, the ERT method makes it possible to reconstruct first-order, lithological, tectonic and gravitational patterns.

Particular first- and second-order gravitational structures are more or less accurately discernible in the ERT profiles in relatively simple slope structures of the MAC and DIC sites. In the case of the MAC, the pattern of initial fissures extending the cave, detected by ERT, suggests the existence of at least two larger subsurface forms (Figs. 2 and 6). The first of these structures comprises an arc-like system of crevices following D_1 and D_2 joint sets which may form amphitheatrical head scarp after potential large-scale gravitational movement. The other structure involves D_1-related westward expanding crevices accurately overlapping elongated surface depressions, which indicates potential future straight-lined scarp development. Geomorphological and speleological observations as well as the ERT analysis at the MAC site proved more or less circular shape of the future main scarps and they point to a rotational (non-structural) type of future gravitational movement, typical of homogenous material or densely jointed rocks, despite structural control (by joint system) of particular sections subject to tension (cave passages).

Contrary to earlier geomorphological and geological observations, geoelectrical analysis of the DIC site indicates much more evident tectonic-lithological conditioning of the slope transformation than in the case of the MAC site (Figs. 3 and 7). The ERT profiles enable interpretation of the lithological diversity of rock massifs and consequent reconstruction of general tectonic-gravitational structures. At the DIC site, the ERT measurement indicates apparent structural control of gravitational-dilation deformations represented by the cave and the landslide. The DIC example also clearly shows shallow landslide forms such as sliding surface and colluvial tongues.

Comparing the MAC and DIC sites, the landslides surrounding the MIC are much more complex with better expression of caves and surficial landforms (Fig. 4A, stages: L1–L7). The ERT profiles using the dipole–dipole configuration enable the identification of the main discontinuity surface (between *in situ* rocks and displaced massif), which is marked by different resistivity patterns above and below the surface and by numerous oval high-resistivity anomalies. This surface is accordingly oriented to rock strata dipping and its spatial position partly overlaps with the MIC bottom measured in several places (Fig. 4B—contour diagrams). Owing to fissure macrodilatancy, main part of the MIC system was formed and gradually developed during successive generation of gravitational movements that segmented the landslide body. Large or dense, well-identified (mapped) galleries of this cave are unequivocally recognized in the ERT images (oval high-resistivity bodies) within the central part of the landslide body (Figs. 4A and 8: G–G′, J–J′, K–K′; Fig. 4A: L3, L4—western part, L5, and L6 stages). However, the analysis of the ERT profiles suggests that relatively deep concentrations of subsurface voids, which are generally zones of lowered rock mass density produced by fissure macrodilatancy, are distributed all over the landslide as well as in the oldest landslide segments (Fig. 4, J–J′ and M–M′ in L1 and L2 stages; Fig. 8, J–J′ and M–M′). They most probably form a complex system of so far inaccessible widened fractures and irregular voids similar to those in the explored MIC. It shows that the already explored MIC is only a part of a system of widened fractures developed close to the extensive landslide sliding zone which is generally flat and characteristic of translational slip.

Besides the MIC, numerous small caves were formed due to dilation within the scarps and trenches of the landslide (Fig. 4A).

These features are observed directly (Fig. 4B) and confirmed by the ERT profiles (Fig. 8). In these profiles (Figs. 4A and 8, J–J′, L–L′, N–N′ and M–M′; Fig. 4A, stages L1, L2, L3 and L7) numerous shallow and relatively small wedge-like or lenticular (of vertical elongation) high-resistivity entities are situated within or close to trenches and escarpments. They represent shallow, secondary dilation zones of widened fractures.

The ERT image reliability was verified by the ERT sounding in profiles with the occurrence of already explored and mapped caves. Moreover, on the basis of the analysis of the H–H′, I–I′ and J–J′ profiles in the lower part of the landslide (Figs. 4 and 8) a new cave has recently been discovered and explored. Dolny Wasserszlog, a discovered cave, is situated within distinct high-resistivity body in the proximity of the crossing of these profiles (Figs. 4A and 8). This 34-m-long cave comprises several narrow passages and a chamber (7 m long, 3 m wide and 2–3 m high) connected to the ground surface by a short narrow shaft (partly dug by cavers). Although it has been the only cave discovered using the ERT profiles so far, it perfectly confirms the reliability of this method.

6. Conclusion

The presented study shows possibilities and limitations of 2D resistivity tomography in the detection of crevice-type caves and other gravitationally induced discontinuities within flysch rock massifs. Although our data set shows reliability of geoelectrical detection of known cavities, a good result is strongly dependent on the choice of an appropriate electrode array. The dipole–dipole electrode array always reveals the position and geometry of known passages and chambers most precisely, whereas the Wenner–Schlumberger and Wenner electrode arrays evidence known structures only roughly. Moreover, related high-resistivity zones may be both vertically and laterally shifted. Shorter electrode spacing eliminates differences in the ERT record when various electrode arrays are used. Suitability of other electrode arrays (e.g. pole–dipole) should be tested for the given phenomena in the future.

The ERT technique brings appropriate results both in the identification of gravitationally induced voids within slopes affected by initial deformations as well as within landslides. In the case of slopes representing the initial stage of gravitational deformations, the ERT analysis is a very effective method enabling the determination of shape and nature of subsurface discontinuities (widened fractures) which form scarps of a potential landslide. In the case of well-developed landslides, the ERT profiles show various types of gravitationally induced subsurface discontinuities and voids, e.g. dilation fractures connected with scarps and trenches as well as zones of voids within landslide bodies formed by complex processes involving fissure macrodilatancy near the sliding zone. The usefulness of ERT measurement as a fast and cost-effective cave-exploration method was verified by the discovery of new passages within the MIC site following our geoelectrical campaign.

Acknowledgement

This research was supported by a project from the Grant Agency of the Czech Republic, No. 205/06/P185: “Comparison of morphotectonics and geomorphic effect of surface uplift in the highest part of the Flysch Western Carpathians and the Crimean Mountains”, partly by a project No. P209/10/0309: “The effect of historical climatic and hydrometeorological extremes on slope and fluvial processes in the Western Beskydy Mts and their forefield” as well as a scientific project No. NN306522738 granted by the Polish Ministry of Sciences in 2010–2013. We gratefully acknowledge Marc Luetscher and an anonymous reviewer for valuable comments which substantially improved the manuscript. Thanks are also extended to Monika Hradecká for her help with text translation and Karel Šilhán, Jan Lenárt, Ondřej Turský, Bartek Juroszek and Grzegorz Szalbot for their assistance during field works.

References

Abu-Shariah, M.I.I., 2009. Determination of cave geometry by using a geoelectrical resistivity inverse model. Engineering Geology 105, 239–244.
Beauvais, A., Parisot, J.C., Savin, C., 2007. Ultramafic rock weathering and slope erosion processes in a South West Pacific tropical environment. Geomorphology 83, 1–13.
Beres, M., Luetscher, M., Olivier, R., 2001. Integration of ground-penetrating radar and microgravimetric methods to map shallow caves. Journal of Applied Geophysics 46, 249–262.
Bichler, A., Bobrowsky, P., Best, M., Douma, M., Hunter, J., Calvert, T., Burns, R., 2004. Three-dimensional mapping of a landslide using a multi-geophysical approach: the Quesnel Forks landslide. Landslides 1, 29–40.
Bober, L., 1984. Landslides in the Polish Flysch Carpathians, and their relation to geology of the region. Biuletyn Instytutu Geologicznego 340, 115–158 (in Polish, with English Abstr.).
Burtan J., Sokołowski S., Sikora W., Żytko K. 1956. Szczegółowa Mapa Geologiczna Polski 1: 50 000, arkusz Milówka. Wyd. Geol. Warszawa. (in Polish).
Burtan, J., 1973. Szczegółowa mapa geologiczna Polski 1: 50 000, arkusz Wisła. Wyd. Geol., Warszawa. (in Polish).
Candansayar, M.E., 2008. Two-dimensional individual and joint inversion of three- and four-electrode array DC resistivity data. Journal of Geophysical Engineering 5, 290–300.
Chambers, J.E., Wilkinson, P.B., Weller, A.L., Meldrum, P.I., Ogilvy, R.D., Caunt, S., 2007. Mineshaft imaging using surface and crosshole 3D electrical resistivity tomography: a case history from the East Pennine Coalfield, UK. Journal of Applied Geophysics 62, 324–337.
Cieszkowski, M., Koszarski A., Leszczyński, S., Michalik, M., Radomski, A., Szulc, J., 1991. Szczegółowa mapa geologiczna Polski 1: 50 000, arkusz Ciężkowice. Wyd. Geol., Warszawa. (in Polish).
Dikau, R., Brunsden, D., Schrott, L., Ibsen, M.L. (Eds.), 1996. Landslide recognition. Identification, Movement and Causes. Willey, Chichester, pp. 1–251.
Drahor, M.G., Göktürkler, G., Berge, M.A., Kurtulmus, T.Ö., 2006. Application of electrical resistivity tomography technique for investigation of landslides: a case from Turkey. Environmental Geology 50, 147–155.
Ezersky, M., 2008. Geoelectric structure of the Ein Gedi sinkhole occurrence site at the Dead Sea shore in Israel. Journal of Applied Geophysics 64, 56–69.
Fazzito, S.Y., Rapalini, A.E., Cortés, J.M., Terrizzano, C.M., 2009. Characterization of Quaternary faults by electric resistivity tomography in the Andean Precordillera of Western Argentina. Journal of South American Earth Sciences 28, 217–228.
Ganerød, G.V., Grøneng, G., Rønning, J.S., Dalsegg, E., Elvebakk, H., Tønnesen, J.F., Kveldsvik, V., Eiken, T., Blikra, L.H., Braathen, A., 2008. Geological model of the Åknes rockslide, western Norway. Engineering Geology 102, 1–18.
Ganszer J., 1997. Jaskinia Malinowska—cross-section. In: Pulina M. (Ed.), Jaskinie polskich Karpat fliszowych, vol. 1. PTPNoZ, Warszawa, appendix. (in Polish).
Ganszer J., Mleczek T., 1997. Diabla Dziura w Bukowcu—map and cross-section. In: Pulina M. (Ed.), Jaskinie polskich Karpat fliszowych, vol. 2. PTPNoZ, Warszawa, appendix. (in Polish).
Godio, A., Strobbia, C., De Bacco, G., 2006. Geophysical characterisation of a rockslide in an alpine region. Engineering Geology 83, 273–286.
Guérin, R., Baltassat, J.M., Boucher, M., Chalikakis, K., Galibert, P.Y., Girard, J.F., Plagnes, V., Valois, R., 2009. Geophysical characterisation of karstic networks—application to the Ouysse system (Poumeyssen, France). Comptes Rendus Geosciences 341, 810–817.
Heincke, B., Günther, T., Dalsegg, E., Rønning, J.S., Ganerød, G.V., Elvebakk, H., 2010. Combined three-dimensional electric and seismic tomography study on the Åknes rockslide in western Norway. Journal of Applied Geophysics 70, 292–306.
Hutchinson, J.N., 1995. Deep-seated mass movements on slopes. Mem. Soc. Geol. It. 50, 147–164.
Jomard, H., Lebourg, T., Tric, E., 2007. Identification of the gravitational boundary in weathered gneiss by geophysical survey: La Clapière landslide (France). Journal of Applied Geophysics 62, 47–57.
Klassek, G., 1997a. Jaskinia Malinowska. In: Pulina, M. (Ed.), Jaskinie polskich Karpat fliszowych, 1. PTPNoZ, Warszawa, pp. 142–146 (in Polish).
Klassek, G., 1997b. Diabla Dziura w Bukowcu. In: Pulina, M. (Ed.), Jaskinie polskich Karpat fliszowych, 2. PTPNoZ, Warszawa, pp. 188–195 (in Polish).
Klassek G., Mleczek T. 2009. Eksploracja i inwentaryzacja jaskiń polskich Karpat fliszowych (wrzesień 2008–sierpień 2009). In: Szelerewicz M., Urban J., Dobrowolski R. (Eds.), Materiały 43. Sympozjum Speleologicznego, 16–18.10.2009, Zamość. Sekcja Speleol. PTP im. Kopernika, Kraków: 62–65. (in Polish).
Kneisel, Ch., 2006. Assessment of subsurface lithology in mountain environments using 2D resistivity imaging. Geomorphology 80, 32–44.
Kranz, R.I., Scholz, C.H., 1977. Critical dilatant volume of rocks at the onset of tertiary creep. Journal of Geophysical Research 82, 4893–4898.
Lapenna, V., Lorenzo, P., Perrone, A., Piscitelli, S., Sdao, F., Rizzo, E., 2003. High-resolution geoelectrical tomographies in the study of Giarrossa landslide (southern Italy). Bulletin of Engineering Geology and Envionment 62, 259–268.
Lexa, J., Bezák, V., Elečko, M., Mello, J., Polák, M., Potfaj, M., Vozár, J. (Eds.), 2000. Geological Map of Western Carpathians and Adjacent Areas 1: 500 000. Geological Survey of Slovak Republic, Bratislava.
Loke, M.H., 1997. Res2DINV Software User's Manual.
Loke, M.H., Barker, R.D., 1996. Rapid least-squares inversion of apparent resistivity 455 pseudosections by a quasi-Newton method. Geophysical Prospecting 44, 131–152.

Maillet, G.M., Rizzo, E., Revil, A., Vella, C., 2005. High resolution electrical resistivity tomography (ERT) in a transition zone environment: application for detailed internal architecture and infilling processes study of a Rhône River paleo-channel. Marine Geophysical Researches 26, 317–328.
Margielewski, W., 2006. Structural control and types of movements of rock mass in anisotropic rocks: case studies in the Polish Flysch Carpathians. Geomorphology 77, 47–68.
Margielewski, W., Urban, J., 2002. Initiation of mass movement in the Polish Flysch Carpathians studied in the selected crevice type caves. In: Rybář, J., Stemberk, J., Wagner, P. (Eds.), Landslides. AA Balkema Publ, Lisse-Abingdon-Exton-Tokyo, pp. 405–409.
Margielewski, W., Urban, J., 2003a. Crevice-type caves as initial forms of rock landslide development in the Flysch Carpathians. Geomorphology 54, 325–338.
Margielewski, W., Urban, J., 2003b. Direction and nature of joints controlling development of deep seated mass movements: a case study of Diabla Dziura cave (Polish flysch Carpathians). Geomorphologia Slovaca 3, 58–59.
Margielewski, W., Urban, J., 2005. Pre-existing tectonic discontinuities in the rocky massifs as initial forms of deep-seated mass movements development: case studies of selected deep crevice-type caves in the Polish Flysch Carpathians. In: Senneset, K., Flaate, K., Larsen, J.O. (Eds.), Landslides and Avalanches ICFL 2005 Norway. Balkema. Taylor and Francis, London, pp. 249–256.
Margielewski, W., Urban, J., Szura, C., 2007. Jaskinia Miecharska cave (Beskid Śląski Mts., Polish Outer Carpathians): case study of a crevice-type cave developed on a sliding surface. Nature Conservation 63, 57–68.
Margielewski, W., Szura, C., Urban, J., 2008. Jaskinia Miecharska cave (Beskid Śląski Mts., Polish Outer Carpathians), the largest non-karst cave in the flysch Carpathians. Zacisk, Special issue 7–13.
Mastella, L., Zuchiewicz, W., Tokarski, A., Rubinkiewicz, J., Leonowicz, P., Szczęsny, R., 1997. Application of joint analysis for palaeostress reconstructions in structurally complicated settings: case study from Silesian Nappe, Outer Carpathians, Poland. Przegląd Geologiczny 45, 1064–1066.
Milsom, J., 2005. Field Geophysics, the Geological Field Guide Series (3rd ed.). Wiley, Chichester. 232 pp.
Nguyen, F., Garambois, S., Chardon, D., Hermitte, D., Bellier, O., Jongmans, D., 2007. Subsurface electrical imaging of anisotropic formations affected by a slow active reverse fault, Provence, France. Journal of Applied Geophysics 62, 338–353.
Otto, J.C., Sass, O., 2006. Comparing geophysical methods for talus slope investigations in the Turtmann valley (Swiss Alps). Geomorphology 76, 257–272.
Poprawa, D., Rączkowski, W., 2003. Carpathian landslide (southern Poland). Przegląd Geologiczny 51, 685–692 (in Polish, with English Abstr.).
Pulina, M., 1997a. Jaskinie polskich Karpat fliszowych, 1. PTPNoZ, Warszawa (in Polish).
Pulina, M., 1997b. Jaskinie polskich Karpat fliszowych, 2. PTPNoZ, Warszawa (in Polish).
Rachwaniec, M., 1997. Jaskinia Malinowska—map. In: Pulina, M. (Ed.), Jaskinie polskich Karpat fliszowych, 1. PTPNoZ, Warszawa. appendix. (in Polish).
Ribolini, A., Guglielmin, M., Fabre, D., Bodin, X., Marchisio, M., Sartini, S., Spagnolo, M., Schoeneich, P., 2010. The internal structure of rock glaciers and recently deglaciated slopes as revealed by geoelectrical tomography: insights on permafrost and recent glacial evolution in the Central and Western Alps (Italy–France). Quaternary Science Reviews 29, 507–521.
Ryłko, W., Paul, Z., 1992. Mapa Geologiczna Polski 1: 200 000 (B—mapa bez utworów czwartorzędowych). Arkusz Cieszyn. Państwowy Instytut Geologiczny, Warszawa.
Sass, O., 2006. Determination of the internal structure of alpine talus deposits using different geophysical methods (Lechtaler Alps, Austria). Geomorphology 80, 45–58.
Sass, O., Bell, R., Glade, T., 2008. Comparison of GPR, 2D-resistivity and traditional techniques for the subsurface exploration of the Öschingen landslide, Schwabian Alb (Germany). Geomorphology 93, 89–103.
Schrott, L., Sass, O., 2008. Application of field geophysics in geomorphology: advances and limitations exemplified by case studies. Geomorphology 93, 55–73.
Starkel, L., 1972. An outline of the relief of the Polish Carpathians and its importance for human management. Problemy Zagospodarowania Ziem Górskich 10, 75–150 (in Polish, with English Abstr.).
Suzuki, K., Toda, S., Kusunoki, K., Fujimitsu, Y., Mogi, T., Jomori, A., 2000. Case studies of electrical and electromagnetic methods applied to mapping active faults beneath the thick quaternary. Engineering Geology 56, 29–45.
Szalai, S., Szarka, L., 2008a. Parameter sensitivity maps of surface geoelectric arrays. Part 1: linear arrays. Acta Geodaetica et Geophysica Hungarica 43, 419–437.
Szalai, S., Szarka, L., 2008b. On the classification of surface geoelectric arrays. Geophysical Prospecting 56, 159–175.
Szalai, S., Novák, A., Szarka, L., 2009. Depth of investigation and vertical resolution of surface geoelectric arrays. Journal of Environmental and Engineering Geophysics 14, 15–23.
Szura, C., 2006. Jaskinia Miecharska—beskidzki gigant. Jaskinie 2 (43), 6 (in Polish).
Szura, C., 2009. Jaskinia Wiślańska—fliszowy gigant w natarciu. Jaskinie 3 (56), 19–21 (in Polish).
Turner, A.K., Schuster, R.L. (Eds.), 1996. Landslides: Investigation and Mitigation. Transportation Research Board, National Academy of Sciences, Washington D.C., Special Report, 247, pp. 391–424.
Van Schoor, M., 2002. Detection of sinkholes using 2D electrical resistivity imaging. Journal of Applied Geophysics 50, 393–399.
Vítek, J., 1983. Classification of pseudokarst forms in Czechoslovakia. Intern. Journ. Speleol. 13, 1–18.
Wagner, J, Demek, J, Stráník, Z., 1990. Jeskyně Moravskoslezských Beskyd a okolí. Knihovna. České speleologické společnosti, Praha. (in Czech).
WP/WLI, 1990. The International Geotechnical Societes UNESCO Working Party for World Landslide Inventory. A suggested method for reporting a landslide. Bulletin of the International Association of Engineering Geology 41, 5–12.
WP/WLI, 1993. The International Geotechnical Societes UNESCO Working Party for World Landslide Inventory. Multilingual Landslide Glossary. The Canadian Geotechnical Society. BiTech Publishers Ltd, Richmond BC, Canada, pp. 1–7.
Zabuski, L., Thiel, K., Bober, L., Zabuski, L., Thiel, K., Bober, L., 1999. Landslides in Polish Carpathian Flysch. Geology–Modeling–Stability calculations. IBW PAN, Gdańsk (in Polish, with English Abstr.).
Zhou, W., Beck, B.F., Stephenson, J.B., 2000. Reliability of dipole–dipole electrical resistivity tomography for defining depth to bedrock in covered karst terranes. Environmental Geology 39, 760–766.
Zhou, W., Beck, B.F., Adams, A.L., 2002. Effective electrode array in mapping karst hazards in electrical resistivity tomography. Environmental Geology 42, 922–928.
Żytko, K., Zając, R., Gucik, S., Ryłko, W., Oszczypko, N., Garlicka, I., Nemčok, J., Eliáš, M., Menčik, E., Stránik, Z., 1989. Map of the tectonic elements of the Western Outer Carpathians and their foreland. PIG Warszawa; GUDS Bratislava; UUG Praha.